# Silicon optical modulator with shield coplanar waveguide electrodes

**Xiaoguang Tu,[1,*] Ka-Fai Chang,[1] Tsung-Yang Liow,[1] Junfeng Song,[1] Xianshu Luo,[1] Lianxi Jia,[1] Qing Fang,[1] Mingbin Yu,[1] Guo-Qiang Lo,[1] Po Dong,[2] and Young-Kai Chen[3]**

[1]*Institute of Microelectronics, A*STAR (Agency for Science, Technology and Research), 11 Science Park Road, Science Park II, 117685, Singapore*
[2]*Bell Labs, Alcatel-Lucent, 791 Holmdel Road, Holmdel, NJ 07733, USA*
[3]*Bell Labs, Alcatel-Lucent, 600 Mountain Avenue, Murray Hill, NJ 07974, USA*
[*]*tux@ime.a-star.edu.sg*

**Abstract:** A silicon Mach-Zehnder Interferometer (MZI) optical modulator with a shield coplanar waveguide (CPW) transmission line electrode design was demonstrated. This shield-CPW electrode suppresses the signal distortion caused by the parasitic slot-line (SL) mode and improves the electrical bandwidth and the electro-optical (EO) bandwidth. With the shield-CPW electrodes and 5.5 mm-long phase shifters, the silicon MZI optical modulator delivered an EO bandwidth of above 24 GHz and a $V_{\pi}$ = 3.0 V was achieved at λ = 1310nm. When modulated at 28-Gb/s data rate, it achieved an extinction ratio of 5.66 dB under a driving voltage of $V_{pp}$ = 1.3 V, corresponding to a power consumption of 0.8 pJ/bit.



**OCIS codes:** (130.3120) Integrated optics devices; (230.7370) Waveguides; (250.7360) Waveguide modulators; (230.3990) Micro-optical devices.

## References and links

1. L. C. Kimerling, D. Ahn, A. B. Apsel, M. Beals, D. Carothers, Y.-K. Chen, T. Conway, D. M. Gill, M. Grove, C.-Y. Hong, M. Lipson, J. Liu, J. Michel, D. Pan, S. S. Patel, A. T. Pomerene, M. Rasras, D. K. I. Sparacin, K.-Y. Tu, A. E. White, and C. W. Wong, "Electronic-photonic integrated circuits on the CMOS platform," Proc. SPIE **6125**, 612502 (2006).
2. M. Paniccia, "Integrating silicon photonics," Nat. Photonics **4**(8), 498–499 (2010).
3. G. T. Reed, G. Mashanovich, F. Y. Gardes, and D. J. Thomson, "Silicon optical modulators," Nat. Photonics **4**(8), 518–526 (2010).
4. T. Y. Liow, J. F. Song, X. G. Tu, E. J. Lim, Q. Fang, N. Duan, M. B. Yu, and G. Q. Lo, "Silicon optical interconnect device technologies for 40Gb/s and beyond," IEEE J. Sel. Top. Quantum Electron. **19**(2), 8200312 (2013).
5. R. A. Soref and B. R. Bennett, "Electrooptical effects in silicon," IEEE J. Quantum Electron. **23**(1), 123–129 (1987).
6. P. Dong, L. Chen, C. J. Xie, L. L. Buhl, and Y. K. Chen, "50-Gb/s silicon quadrature phase-shift keying modulator," Opt. Express **20**(19), 21181–21186 (2012).
7. D. J. Thomson, F. Y. Gardes, J. M. Fedeli, S. Zlatanovic, Y. F. Hu, B. P. P. Kuo, E. Myslivets, N. Alic, S. Radic, G. Z. Mashanovich, and G. T. Reed, "50-Gb/s Silicon Optical Modulator," IEEE Photon. Technol. Lett. **24**(4), 234–236 (2012).
8. X. G. Tu, T. Y. Liow, J. F. Song, X. S. Luo, Q. Fang, M. B. Yu, and G. Q. Lo, "50-Gb/s silicon optical modulator with traveling-wave electrodes," Opt. Express **21**(10), 12776–12782 (2013).
9. M. Streshinsky, R. Ding, Y. Liu, A. Novack, Y. S. Yang, Y. J. Ma, X. G. Tu, E. K. Chee, A. E. Lim, P. G. Lo, T. Baehr-Jones, and M. Hochberg, "Low power 50 Gb/s silicon traveling wave Mach-Zehnder modulator near 1300 nm," Opt. Express **21**(25), 30350–30357 (2013).
10. X. Xiao, H. Xu, X. Y. Li, Z. Y. Li, T. Chu, Y. D. Yu, and J. Z. Yu, "High-speed, low-loss silicon Mach-Zehnder modulators with doping optimization," Opt. Express **21**(4), 4116–4125 (2013).
11. P. Dong, X. Liu, C. Sethumadhavan, L. L. Buhl, R. Aroca, Y. Baeyens, and Y. K. Chen, "224-Gb/s PDM-16-QAM Modulator and Receiver based on Silicon Photonic Integrated Circuits," OFC/NFOEC, PDP5C.6 (2013).
12. K. Goi, A. Oka, H. Kusaka, Y. Terada, K. Ogawa, T. Y. Liow, X. G. Tu, G. Q. Lo, and D. L. Kwong, "Low-loss high-speed silicon IQ modulator for QPSK/DQPSK in C and L bands," Opt. Express **22**(9), 10703–10709 (2014).
13. S. Assefa, S. Shank, W. Green, M. Khater, E. Kiewra, C. Reinholm, S. Kamlapurkar, A. Yang, J. Proesel, J. Hofrichter, B. Offrein, X. X. Gu, W. Haensch, J. E. Monaghan, and Y. Vlasov, "A 90nm CMOS Integrated Nano-Photonics Technology for 25Gbps WMD Optical Communications Applications," IEDM12–809 (2012).

#215239 - $15.00 USD Received 8 Jul 2014; revised 18 Aug 2014; accepted 19 Aug 2014; published 19 Sep 2014

14. T. Takemoto, F. Yuki, H. Yamashita, S. Tsuji, Y. Lee, K. Adachi, K. Shinoda, Y. Matsuoka, K. Kogo, S. Nishimura, M. Nido, M. Namiwaka, T. Kaneko, T. Sugimoto, and K. Kurata, "100-Gbps CMOS transceiver for multilane optical backplane system with a 1.3 cm$^2$ footprint," Opt. Express **19**(26), B777–B783 (2011).
15. K. P. Ma, Y. X. Qian, and T. Itoh, "Analysis and applications of a new CPW-Slotline Transition," IEEE. Trans. Microwave. Theory. Tech. **47**, 426–432 (1999).
16. H. Xu, X. Y. Li, X. Xiao, Z. Y. Li, Y. D. Yu, and J. Z. Yu, "Demonstration and characterization of high-speed silicon depletion-mode Mach-Zehnder modulators," IEEE J. Sel. Top. Quantum Electron. **20**(4), 3400110 (2014).
17. N. I. Dib, P. B. Katehi, and G. E. Ponchak, "Analysis of shielded CPW discontinuities with air-bridges," IEEE. MTT S **45**, 469–472 (1991).
18. Z. J. Chen, A. Megrant, J. Kelly, R. Barends, J. Bochmann, Y. Chen, B. Chiaro, A. Dunsworth, E. Jeffrey, J. Y. Mutus, P. J. J. Omalley, C. Neill, P. Roushan, D. Sank, A. Vainsencher, J. Wenner, T. C. White, A. N. Cleland, and J. M. Martinis, "Fabrication and characterization of aluminum air-bridges for superconducting microwave circuits," Appl. Phys. Lett. **104**(5), 052602 (2014).
19. K. Kawano, T. Kitoh, H. Jumonji, T. Nozawa, and M. Yanagibashi, "New travelling-wave electrode Mach-Zehnder optical modulator with 20 GHz bandwidth and 4.7 V driving voltage at 1.52 μm wavelength," Electron. Lett. **25**(20), 1382–1383 (1989).
20. W. R. Eisenstadt and Y. S. Eo, "S-Parameter-Based IC Interconnect transmission line characterization," IEEE. Trans. Compon. Hybr. **15**(4), 483–490 (1992).
21. K. Kawano, T. Kitoh, O. Mitomi, T. Nozawa, and H. Jumonji, "A wide-band and low-driving-power phase modulator employing a Ti: $LiNbO_3$ optical waveguide at 1.5 μm wavelength," IEEE Photon. Technol. Lett. **1**(2), 33–34 (1989).
22. X. G. Tu, T. Y. Liow, J. F. Song, M. B. Yu, and G. Q. Lo, "Fabrication of low loss and high speed silicon optical modulator using doping compensation method," Opt. Express **19**(19), 18029–18035 (2011).
23. P. Dong, L. Chen, and Y. K. Chen, "High-speed low-voltage single-drive push-pull silicon Mach-Zehnder modulators," Opt. Express **20**(6), 6163–6169 (2012).
24. H. T. Chen, "Development of an 80-Gbit/s InP-based Mach-Zehnder Modulator," Ph. D. Dissertation, Dept. Elect. Eng. Comput. Sci., Technical Univ., Berlin, Germany. 65–66 (2007).

## 1. Introduction

The emerging silicon photonics technology has received intense research and development efforts by the optical communication industry due to its superior advantages such as small die sizes, low cost and high integration capability [1–4]. Silicon modulator is one of the most important components for high quality and large volume of data uploading in the future fiber-optic network. Since the comprehensive study of electro-optical (EO) effect in silicon material in 1987 [5], silicon EO modulator has achieved remarkable progress. Recently with reverse-biased p-n junction, the data rate of silicon optical modulator has reached over 50-Gb/s for both of 1310 nm and 1550 nm [6–10]. The aggregated data rate and modulation efficiency may be further increased by utilizing the amplitude-shift keying (ASK) and phase-shift keying (PSK) technologies [11, 12]. Chip-scale integration of silicon modulators with wavelength-division multiplexing (WDM) multiplexers as well as III-V lasers were also demonstrated [13, 14].

For all practical applications, low power consumption and driving voltage are critical performance requestment. That is why in the past, optical modulator fabricated by $LiNbO_3$ and compound material was usually made to have a long phase shifting length. However, such long phase shifter also introduces high microwave loss and velocity mismatching which limit the EO bandwidth. Typically, travelling-wave electrode is implemented to reduce the driving voltage while maintain high EO bandwidth. Coplanar waveguide (CPW) and slot-line (SL) waveguide are two of the most common travelling-wave electrode designs. Between them, CPW is more popular for the advantages of low dispersion, low radiation and the ease of shunt and series connections. However, SL mode can be triggered by the asymmetric CPW electrodes, which in turn becomes the main obstacle for its implementation in practice [15]. When applying CPW electrodes onto optical modulator, the parasitic SL mode can induce strong microwave reflection which suppresses the bandwidth of the modulator. A simple wire-bonding method has been utilized to eliminate this parasitic SL mode [16], but it is not effective and also this approach is not compatible with CMOS process [17]. An air bridge technique, where a shield metal layer is added on top of CPW, has been demonstrated to be more effective for suppressing of this parasitic SL mode [18]. Based on this, shield-CPW

#215239 - $15.00 USD Received 8 Jul 2014; revised 18 Aug 2014; accepted 19 Aug 2014; published 19 Sep 2014
 

electrode has been utilized on $LiNbO_3$ modulators [19]. Nevertheless, there is no report on applying this shield-CPW electrode on silicon modulators.

In this work, we implemented a shield-CPW electrode to suppress the unwanted SL modes in silicon modulator. For illustration, with a 5.5 mm-long phase shifter, the driving voltage $V_{pp}$ is reduced to be less than 1.3 V in a single-end MZI silicon modulator to achieve a 28-Gb/s data rate and above 24 GHz EO-$S_{21}$ −3 dB bandwidth with a power consumption of 0.8 pJ/bit.

## 2. Simulation of shield CPW travelling-wave electrodes

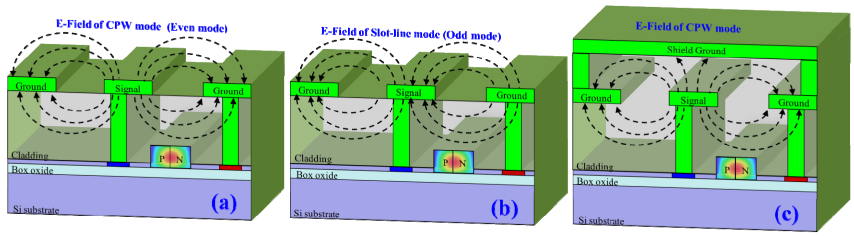


Fig. 1. E-field distributions of microwave modes travel in the travelling-wave electrodes. (a) CPW mode travelling in the conventional CPW electrode. (b) SL mode travelling in the conventional CPW electrode. (c) CPW mode travelling in the shield-CPW electrode.

Figs. 1(a) and 1(b) show the electrical-field (E-field) distribution of the microwave modes travelling in the conventional CPW transmission line. The fundamental mode travelling in the conventional CPW is a hybrid mode of CPW mode (even mode) and SL mode (odd mode). The CPW mode has symmetric voltage distribution while the SL mode has asymmetric distribution on the two ground electrodes. In conventional CPW circuits, the two slots cannot always be kept to the same length and a mode conversion from CPW mode to SL mode often occurs. This is undesirable since it may degrade the performance of the CPW optical modulator. Meanwhile, in shield-CPW transmission line, a shield ground metal is utilized to equalize the voltage of the two ground electrodes. The corresponding E-field distribution is shown in Fig. 1(c). With the suppression of the coupled SL mode, only does the CPW mode propagate in this transmission line.

The microwave performances of silicon phase shifters with CPW and shield-CPW transmission line were simulated by Agilent's Advanced Design System (ADS) with the effective circuit model shown in Fig. 2. A 5.5 mm-long phase shifter is equally divided into 10 unit cells and the shield ground metal is simulated by an inductance (L) between the two ground lines. Two terminals with 50 ohm impedance are added at the two ends of the transmission lines. The simulation structure is set up according to the cross-section of the silicon phase shifter. In the unit cell of the phase shifter, C and R denote the p-n junction capacitance and series resistance between the contact and the p-n junction respectively. We choose the unit length of 550 μm, with a 10 μm center metal line width and 6.4 μm gaps between the metal lines. The loaded capacitance is C = 0.1925 pF, the series resistance is R = 0.385 Ω and the inductance is L = 0.1 nH. These parameters are chosen randomly in order to show the effect of the shield metal layer. The frequency scan range was set from 0 to 40 GHz with a step size of 0.25 GHz.

#215239 - $15.00 USD Received 8 Jul 2014; revised 18 Aug 2014; accepted 19 Aug 2014; published 19 Sep 2014
 

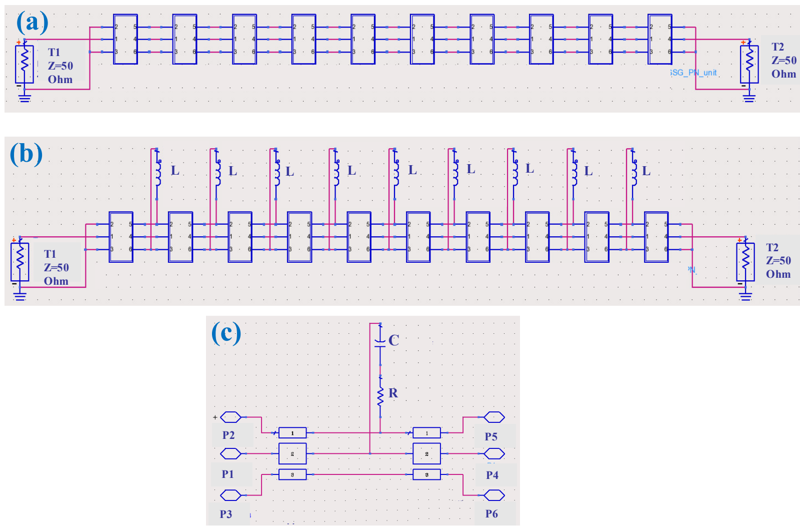


Fig. 2. Effective circuit models of the phase shifters. (a) Conventional CPW transmission line. (b) Shield-CPW transmission line. (c) The unit cell of the phase shifter in (a) and (b).

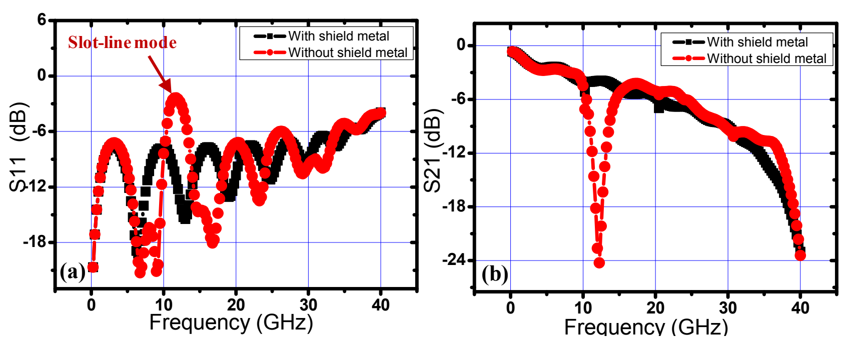


Fig. 3. Simulated electrical S-parameters of the silicon phase shifter with conventional CPW (red color) and shield-CPW transmission line (black color). (a) EE-$S_{11}$ denotes the reflection coefficient. (b) EE-$S_{21}$denotes the transmission coefficient.

The simulated electrical S-parameters (EE S-parameter) of the conventional CPW and shield-CPW electrodes are shown in Fig. 3. In the conventional CPW electrode, the parasitic SL mode induces a strong reflection (EE-$S_{11}$) around 11.8 GHz in Fig. 3(a) which degrades the transmission coefficient (EE-$S_{21}$) at the same frequency as shown in Fig. 3(b). According to the basic transmission line theory, EE-$S_{11}$ has a periodic relationship with frequency which largely depends on the propagation constant of the microwave mode [20]. In Fig. 3(a), it is apparent that EE-$S_{11}$ has a uniform reflection period for the shield-CPW electrodes case, which indicates that only one mode travels in the transmission line. However, two different periods are observed in the EE-$S_{11}$ curve obtained from the conventional CPW transmission line. This indicates the existence of two modes which are CPW mode and SL mode respectively. The SL mode is removed by the shield ground metal layer in the shield-CPW transmission line and thus the corresponding strong reflection disappears. With this shield metal layer, the EE-$S_{21}$ of the conventional CPW is optimized and a higher EO bandwidth can be expected. Once the travelling velocity of the microwave in the shield-CPW transmission line can be further optimized in order to meet with that of the optical-wave travels in the silicon waveguide, a lower driving voltage can be achieved simultaneously. Similar approach has been demonstrated previously in the case of $LiNbO_3$ modulators [21].

## 3. Device fabrication

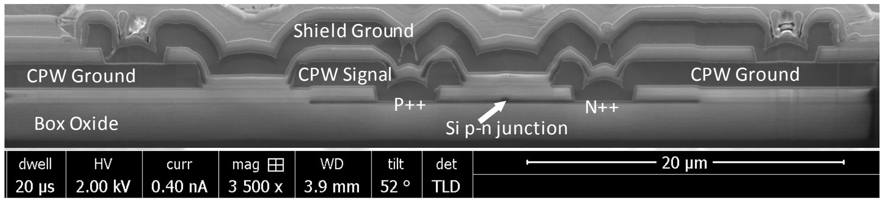


Fig. 4. Cross-section of the modulator phase shifter with shield-CPW transmission line.

Figure 4 shows the cross-section view of the fabricated phase shifter with shield-CPW transmission line. SOI wafers with 220 nm top silicon and 3 µm buried oxide were used. The phase shifter consists of a p-n junction with 100 nm slab thickness. After the oxide cladding deposition and via open, a first 2 µm Aluminum layer were deposited and patterned. After a 1.2 µm oxide cladding and second via open, the second 2 µm Aluminum layer was deposited and patterned for the shield ground. A compensated doping method was utilized to optimize the doping profile of PN junction for high speed and low phase shifter loss [8, 22]. To ensure operating in a single mode condition, the width of the waveguide was chosen to be ~410 nm and 500 nm for λ = 1310 nm and λ = 1550 nm respectively. The fabrication of the silicon modulator is compatible with standard CMOS process.

## 4. Experimental results and discussion

### *4.1 Modulator efficiency at λ = 1310 nm and λ = 1550 nm*

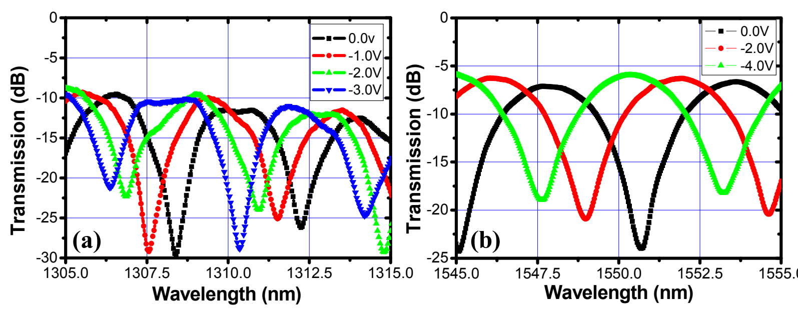


Fig. 5. Measured output spectra of silicon modulator with shield-CPW electrode at (a) λ = 1310 nm and (b) λ = 1550 nm.

**Table 1. The benchmarking table of silicon optical modulator.**

| Wavelength (nm) | $V_\pi$ (V) | $V_\pi L_\pi$ (V·cm) | Phase shifter loss (dB/mm) | Phase shifter Insertion loss (dB) | $V_\pi \cdot L_\pi \cdot$Loss (V·dB) | Ref |
|---|---|---|---|---|---|---|
| 1550 | 28.0 | 2.80 | −3.20 | −3.20 (1.0mm) | 89.6 | Ref [7] |
| 1310 | 8.10 | 2.43 | −1.11 | −3.34 (3.0mm) | 27.0 | Ref [9] |
| 1550 | 27.3 | 2.05 | −1.60 | −1.20 (0.75mm) | 32.8 | Ref [10] |
| 1550 | 18.0 | 1.80 | −2.80 | −2.80 (1.0mm) | 50.4 | Ref [16] |
| 1550 | 3.1 | 1.86 | −1.20 | −7.2 (6.0mm) | 22.3 | Ref [23] |
| 1310 | **3.0** | **1.65** | −1.39 | −7.65 (5.5mm) | **22.9** | This work |
| 1550 | **4.0** | **2.20** | −0.94 | −5.17 (5.5mm) | **20.7** | This work |

The measured output spectra of the silicon modulator under different bias voltage $V_{bias}$ are shown in Fig. 5. The free spectrum range (FSR) of the asymmetric MZI is $FSR_{1310}$ = 3.84 nm and $FSR_{1550}$ = 4.58, corresponding to a group index ($N_g$) of $N_{g.1310}$ = 4.47 and $N_{g.1550}$ = 4.37. A $V_{\pi.1310}$ = 3.0 V and $V_{\pi.1550}$ = 4.0 V are realized with a 5.5 mm-long phase shifter, corresponding to a modulation efficiency of $V_\pi \cdot L_\pi$ of 1.65 V· cm and 2.20 V· cm,

#215239 - $15.00 USD Received 8 Jul 2014; revised 18 Aug 2014; accepted 19 Aug 2014; published 19 Sep 2014
 

respectively. The phase shifter loss includes the free-carriers absorption loss and the loss coming from the sidewall roughness of the waveguide. The passive waveguide loss contributes −0.42 dB/mm of the −1.39 dB/mm phase shifter loss at λ = 1310 nm and −0.25 dB/mm of the −0.94 dB/mm phase shifter loss at λ = 1550 nm. The $V_{\pi} \cdot L_{\pi} \cdot$ Loss figure-of-merit is better than that reported previously, as summarized in Table 1.

*4.2 Electrical S-parameters between CPW and shield-CPW transmission lines*

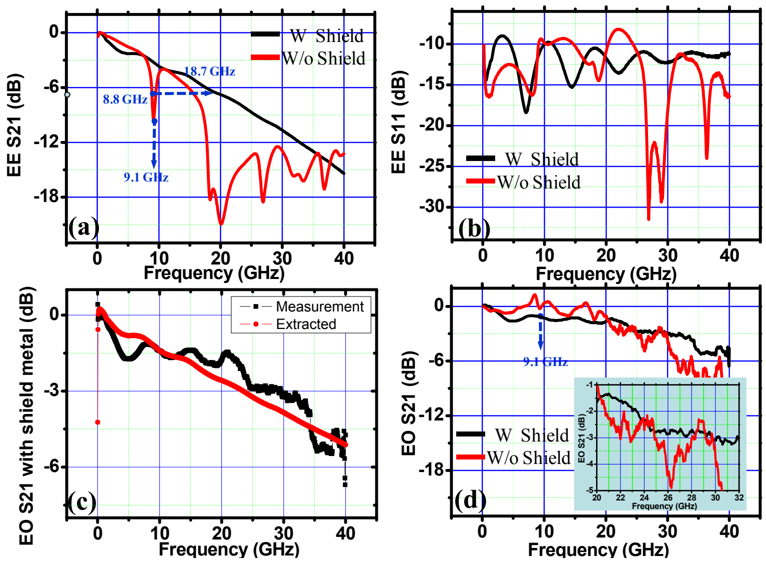


Fig. 6. Measured S-parameters of a 5.5 mm-long phase shifter under $V_{bias}$ = −5.0 V and λ = 1310 nm. (a) Electrical transmission coefficient EE-$S_{21}$. (b) Electrical reflection coefficient EE-$S_{11}$. (c) Measured and extracted Electro-Optical transmission coefficient EO-$S_{21}$ with shield-CPW electrodes. (d) EO-$S_{21}$ with a magnified image of the EO-$S_{21}$ −3 dB point.

Small signal performance of the microwave travelling in the electrodes are measured by Agilent N4373C Lightwave Component Analyzer. The 2-port S-parameters measurement is performed with Cascade high speed probes calibrated with standard short-open-load-through method.

A travelling wave Mach-Zehnder modulator can be treated electrically as a transmission line and the EO bandwidth is defined as the frequency, for which the optical intensity modulation depth has fallen to 70.7% of the reference level, causing a 3 dB reduction in the received signal. Under both of perfect impedance match and perfect velocity match condition, in order to achieve a 3 dB reduction in the received optical signal; the calculated electrical loss is −6.4 dB. However in most of the real cases, the electrodes have some loss and neither the impedance nor the velocity is perfect matched. In that case, the EO-S parameters can be exacted from EE-S parameters [24]. The S-parameters of conventional CPW and shield-CPW electrodes are shown in Fig. 6. In Fig. 6(a), the EE-$S_{21}$ curve becomes much smoother in shield-CPW electrode without any dips. As a result, the −6.4 dB bandwidth is increased from 8.8 GHz to 18.7 GHz. On the EE-$S_{11}$ curve in Fig. 6(b), the strong reflection around high frequency is pulled down to below −10 dB in the shield-CPW electrode. At low frequency, the reflection is increased comparing with the conventional CPW electrode because of the impedance mismatch. The design of the shield metal structures still needs optimization which will be explained later.

With the measured EE-S parameters, the RF loss and effective index of the microwave can be achieved and the EO-$S_{21}$ of the shield-CPW electrodes is extracted as shown in Fig. 6(c). The measured EO-$S_{21}$ curve fits well with the extracted curve. The measured EO-$S_{21}$ of conventional CPW and shield-CPW electrodes are shown in Fig. 6(d) with a magnified image

#215239 - $15.00 USD Received 8 Jul 2014; revised 18 Aug 2014; accepted 19 Aug 2014; published 19 Sep 2014

of the EO-$S_{21}$ −3 dB point. It shows that the shield metal electrodes dose help to clean the unwanted modes and improve the EO-$S_{21}$ −3 dB bandwidth from 22 GHz to 30 GHz. The measured EO-$S_{21}$ −3 dB bandwidth is higher than the EE-$S_{21}$ −6.4 dB bandwidth because of the measurement error at the low frequency part. Here we compare the performance of the conventional CPW and shield-CPW transmission line at λ = 1310 nm. Similar condition happens at λ = 1550 nm.

*4.3 Electrical eye-diagrams of silicon modulator with shield-CPW electrode*

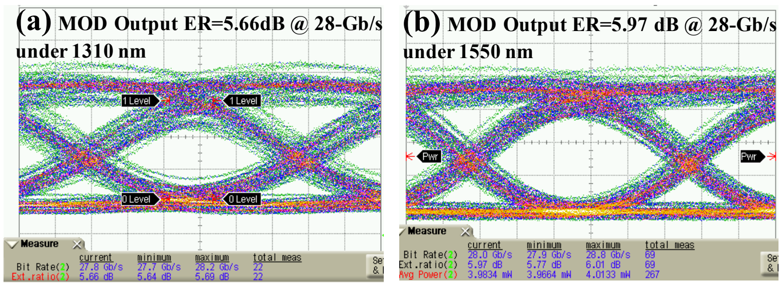


Fig. 7. Measured eye-diagrams of silicon modulator with shield-CPW electrode under $V_{bias}$ = −5 V and $V_{pp}$ = 1.3 V. (a) λ = 1310 nm. (b) λ = 1550 nm.

Large signal testing was performed on the silicon optical modulator using a 50/56-Gbit/s Anritsu Pattern Generator MP1822A and a 60 GHz DC bias tee with a 67 GHz probe. A 50 Ohm resistor was connected on the other end of the travelling-wave electrodes for termination. The continuous-wave light coming from the tunable laser was modulated by adding a non-return-zero pseudorandom binary sequence (PRBS) $2^{31}$-1 signal under $V_{bias}$ = −5.0 V with $V_{pp}$ = 1.3 V. The output optical signal was amplified and collected by an Agilent DCA after an optical band pass filter. At a data rate of 28-Gb/s, extinction ratios of 5.66 dB and 5.97 dB at λ = 1310 nm and λ = 1550 nm are achieved, as shown in Fig. 7(a) and Fig. 7(b). The measured power consumption is 0.8 pJ/bit and 1.1 pJ/bit for λ = 1310 nm at λ = 1550 nm.

## 5. Further optimization of the shield-CPW electrodes

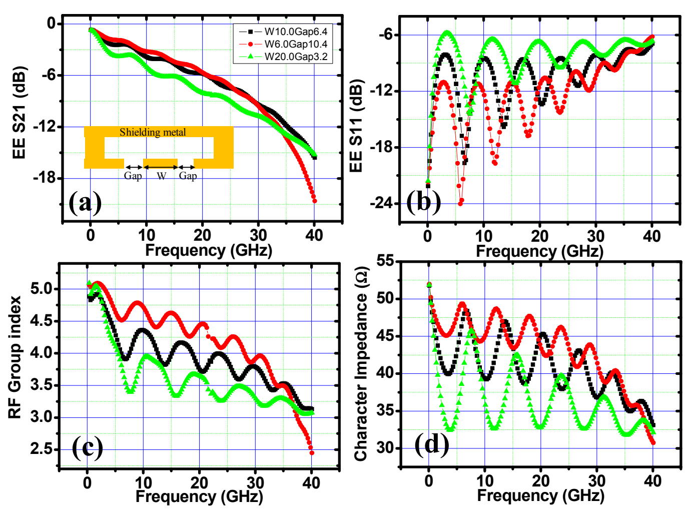


Fig. 8. Simulated microwave performance of the phase shifter with shield-CPW electrodes include (a) EE-$S_{21}$, (b) EE-$S_{11}$, (c) Group index and (d) Character impedance under case (1) W = 10.0 µm and Gap = 6.4 µm (black curve), case (2) W = 6.0 µm and Gap = 10.4 µm (red curve) and case (3) W = 20.0 µm and Gap = 3.2 µm (green curve).

#215239 - $15.00 USD Received 8 Jul 2014; revised 18 Aug 2014; accepted 19 Aug 2014; published 19 Sep 2014

Since the SL mode is suppressed, the only microwave mode travelling in the shield-CPW electrodes is the CPW mode. In order to further improve the performance of the silicon modulator, three width and gap sizes of the CPW line are chosen to simulate the performance of the shield-CPW electrode with case (1): W = 10.0 μm and Gap = 6.4 μm; case (2): W = 6.0 μm and Gap = 10.4 μm and case (3): W = 20.0 μm and Gap = 3.2 μm. Case (1) is what we used in the above experiment. The simulation results are shown in Fig. 8.

Comparing three electrode design cases, case (2) has a similar EE-$S_{21}$ curve with case (1) in Fig. 8(a), but has a lower EE-$S_{11}$ curve in Fig. 8(b). This indicates that the microwave reflection can be reduced by using the shield-CPW with smaller W and larger Gap size. The group index of case (2) as shown in Fig. 8(c) is matching with optical mode whose group index is around 4.47. The corresponding impedance of case (2) is also closer to 50 ohms in Fig. 8(d). This will contribute to a lower driving voltage. Case (3) has a lower group index and impedance, and is the worst one in the 3 cases. In our current fabrication, we used case (1), but from the simulation results, case (2) would be a better choice.

It has to be noted that application of shield-CPW transmission line has some limitation. The strong reflection of SL mode can take place at any frequency, depending on the characteristics of the SL mode and especially the length of the electrode. In short CPW transmission lines, this frequency value can be quite high. Hence the shield-CPW method will contribute little to the improvement of EO-$S_{21}$ bandwidth. However, in the case that a long phase shifter is chosen to achieve a low driving voltage, the shield-CPW electrodes will be useful. The same approach can be utilized to improve travelling-wave photo-detectors.

## 6. Conclusion

We demonstrated a 5.5 mm-long silicon optical modulator with shield-CPW electrode. The shield metal layer suppressed the parasitic SL modes such that both the EO bandwidth and driving voltage of the silicon modulator are improved. A 28-Gb/s data rate, $V_\pi$ of 3.0 V and 4.0 V are demonstrated at $\lambda$ = 1310 nm and $\lambda$ = 1550 nm respectively. Combining long phase shifter sections with improved shield-CPW electrode design, low $V_\pi$ operations can be expected with higher modulation speed. This is in line with advanced ASK and PSK modulation formats for the future high capacity low power OEICs with low power requirements.

## Acknowledgment

This research is based upon work supported in part by the Office of the Director of National Intelligence (ODNI), Intelligence Advanced Research Projects Activity (IARPA), via Sandia National Laboratories. The views and conclusions contained herein are those of the authors and should not be interpreted as necessarily representing the official policies or endorsements, either expressed or implied, of ODNI, IARPA, or the U.S. Government. The U.S. Government is authorized to reproduce and distribute reprints for Governmental purposes notwithstanding any copyright annotation thereon.